Tribology Letters (2022) 70: 71
https://doi.org/10.1007/s11249-022-01604-4

ORIGINAL PAPER

Compositional Tuning Reveals a Pathway to Achieve a Strong and Lubricious Double Network in Agarose-Polyacrylamide Hydrogels

Tooba Shoaib[1] · Paige Prendergast[1] · Rosa M. Espinosa-Marzal[1,2]

Received: 10 February 2022 / Accepted: 17 April 2022 / Published online: 24 May 2022
© The Author(s), under exclusive licence to Springer Science+Business Media, LLC, part of Springer Nature 2022

Abstract

Hydrogels, bearing microstructural semblance to biological tissues, are prime candidates for translation replacement materials. Among them, double network (DN) hydrogels are at the forefront with their superior mechanical properties compared to conventional single network hydrogels. However, the functional design of the microstructure to control mechanical and tribological performance still poses a challenge. Here, hydrogels composed of physically crosslinked agarose and chemically crosslinked poly(acrylamide) were studied by spectroscopy, dynamic light scattering, atomic force microscopy and rheology. A viable hydrogel formed with the lowest acrylamide concentration, but the loose PAAm network did not reinforce the agarose network. Increasing the monomer and crosslinker concentration led to fast gelation of the second network, yielding poorly interconnected acrylamide-rich domains within the agarose network, and a weak and heterogenous hydrogel. Reducing the crosslinking degree to the half slowed down gelation, which favored the formation of an interpenetrating PAAm network, affording a two-fold increase in strength. While the adhesion of the investigated hydrogels is remarkably dictated and reduced by agarose, their frictional characteristics are highly sensitive to the composition. Importantly, friction can be modulated by varying the imbibed fluid.

Keywords Hydrogels · Friction · Biolubrication · Agarose · Polyacrylamide · Double networks

1 Introduction

Hydrogels are proposed as prime candidates for cartilage replacement owing to their structural semblance to biological tissues, their functionality, and biocompatibility [1, 2]. One outstanding challenge is to design hydrogels with excellent biomechanical response along with the capability to reduce wear and friction. For instance, articular cartilage maintains structural integrity under cyclic loading and unloading during which the pressures can rise up to 20 MPa [3]. However, conventional chemically crosslinked single network hydrogels can sustain pressures up to only ~ 0.4 MPa before yield or fracture [4, 5]. Single network hydrogels are weak and brittle [6, 7] and their fracture strengths are orders of magnitudes lower than those of human tissues [8] Hence, the disparity between hydrogels' mechanical properties and those of soft biological tissues such as the articular cartilage is still a vital limitation.

In 2003, Gong pioneered the so-called double network hydrogels, where a polyelectrolyte, poly(2-acrylamido-2-methylpropane sulfonic acid), (abbrev. PAMPS), as the first network, was tightly crosslinked and brittle, and the second network, poly(N,N'-dimetyl acrylamide (abbrev. PDMAAm) was loosely crosslinked, soft, ductile, and neutral [9–12]. These hydrogels have strength and toughness comparable to articular cartilage and industrial rubber [4, 13]. Nakajima et al. demonstrated that two different types of networks are possible: truly independent (t-DN) and connective (c-DN) hydrogels [14] DN hydrogels with PAMPS as the first network when crosslinked with methylene bisacrylamide can lead to unreacted double bonds in the crosslinker. These double bonds can react with the second network's pre-polymer, resulting in covalent links between first and second network, i.e., c-DN hydrogels. By rendering all the unreacted double bonds inert, the authors were able to synthesize

✉ Rosa M. Espinosa-Marzal
roase@illinois.edu

[1] Department of Materials Science and Engineering, University of Illinois at Urbana-Champaign, Urbana, IL 61801, USA

[2] Department of Civil and Environmental Engineering, University of Illinois at Urbana Champaign, Urbana, IL 61801, USA

two independent, interpenetrating networks, *i.e.* t-DN hydrogels. Importantly, the authors found that the t-DN gels were stronger than the c-DN gels when the second network was loosely cross-linked. For other systems, it has been shown that [15] when the concentration of the cross-linking monomer used in the second polymerization was below some critical value, the toughness of a c-DN was higher than that of a t-DN, but above some critical cross-linker concentration, the toughness of the t-DN improved remarkably. It should be noted that authors in ref [15]. point out the validity of a "double" network if the two polymers are interconnected, implying that it is essentially a single crosslinked network in the c-DN case. Several works have shown that the amount of monomer and crosslinker of the second network significantly influences the resulting microstructure and properties of the hydrogel [8, 16–22] and that a fine balance is required to achieve extraordinary property enhancements. Other network combinations have had success in achieving improved mechanical properties. For instance, a physically crosslinked first network like agarose [22–24], collagen [25, 26], or alginate [27, 28], can eliminate the damage associated with the covalently crosslinked first network in DN hydrogels.

Yet, this discovery came with a caveat; Gong's studies noted that a third component was necessary to achieve low friction coefficients [29]. For example, the friction coefficient provided by PAMPS/PAAm DN hydrogel ranged from 10^{-2}–10^{-1}, while high lubricity ($\mu \sim 10^{-5}$) was only achieved if a linear, un-crosslinked polymer was imbibed in the DN hydrogel. The authors attributed the low coefficients of friction to the shear of free and highly mobile linear polymer chains at the hydrogel interface. Studies of DN hydrogel lubrication are still limited but the available studies have often revealed poor lubrication [9, 16, 20, 29–31]. For instance, polyvinyl alcohol (PVA)/poly(acrylamide) (PAAm)hydrogels showed friction coefficients as high as ~ 0.1–0.2 in migrating and stationary contacts. [20] Later studies have revealed lower friction coefficients (μ~10^{-2}–10^{-3}) for DN hydrogels comprising PAMPS/PDMAAm [16] and alginate/PAAm [27], but the knowledge of the underlying mechanisms and the structure–property relationships for enhanced lubricity are almost non-existent. Recently, Bonyadi et al. showed that a charged first network could render superlubricity to PAMPS/poly(N-isopropylacrylamide-co-acrylamide) DN hydrogel at low velocities, which was associated with a fluid film preventing the contact between the sliding surfaces [32]. Chemical gradients in DN hydrogels can also influence the frictional response [31]. For example, DN hydrogels composed of alginate and PAMPS showed an alginate-rich skin, which could be easily delaminated, revealing a softer hydrogel underneath the skin with a lower friction coefficient. The authors attributed the presence of gradients to the oxygen inhibited free-radical polymerization and to the diffusion-controlled crosslinking of alginate within the double network.

We have studied agarose/polyacrylamide hydrogels (Ag-PAAm) composed of agarose, as the first (physically crosslinked) network, and PAAm, as the second (chemically crosslinked) network. Although promising due to the ease of synthesis, charge neutrality and biocompatibility [17], the fundamentals about the formation of an efficient double network are still paradoxical, and the knowledge of the relation between microstructure and lubrication performance is lacking, both limiting their functionality. Agarose is a neutral polysaccharide that is extracted from red algae; its molecular structure consists of two alternating galactose types. Gelation occurs by cooling a solution of agarose below the ordering temperature (~ 32 ºC). During gelation, the conformational transition of the two coils to a double helix is followed by the aggregation of the double-helical segments via hydrogen bonding and van der Waals forces. The gelation of PAAm in the agarose network is modulated by varying monomer and crosslinker concentrations. Here, we systematically modified the second network's composition (PAAm) and determined the microstructure, strengthening, adhesion and frictional characteristics in various solvents. These results provide insight into the principles underlying the formation of a double network with enhanced mechanical and tribological performance.

2 Experimental Section/Methods

2.1 Hydrogel Preparation

All chemicals were purchased from Millipore-Sigma (MO, USA) unless otherwise noted. The hydrogels were prepared with solutions of agarose powder (1st network prepolymer), acrylamide (2nd network monomer), bis-acrylamide (2nd network crosslinker), α-Ketoglutaric acid (2nd network UV initiator). A UV lamp from Spectroline (USA) with an optimal wavelength of 365 nm was used. The synthesis method was adapted from the protocol reported in ref. [22] In brief, 1 wt% agarose powder was added to pre-heated DI water to 80 ºC under constant stirring. After 10 min, the solution became clear (indicative of agarose dissolution), and acrylamide (AAm) and bis-acrylamide (bis-AAm) were added to the agarose solution to a total volume of 20 mL, followed by the initiator. After stirring for 10 s, 2 ml were pipetted into a polycarbonate petri dish. Agarose gelation was allowed to occur for 30 min, after which the samples were put under UV light for 4 h for the second network to form. Lastly, the gels were thoroughly washed to remove unreacted components. Four different hydrogels were prepared with the compositions given in Table 1. Note that the difference

Table 1 Composition of synthesized Ag-PAAm hydrogels

Hydrogels prepared with 1wt% agarose	Water with agarose (mL)	Water with AAm + bis-AAm (mL)	AAm (wt%)	bis-AAm (wt%)
1Ag4PAAm-0.1x	14.7	5.3	4.0	0.10
1Ag5PAAm-0.15x	16	4	5.0	0.15
1Ag5PAAm-0.3x	14.5	5.5	5.0	0.30
1Ag8PAAm-0.48x	11.2	8.8	8.0	0.48

For all hydrogels, the amount of the UV initiator was 1 mol% of the AAm monomer. All hydrogel solutions were made up to a total volume of 20 mL, by mixing agarose and acrylamide solutions. The concentrations of agarose, AAm and bis-AAm refer to the total volume of 20 mL

between 1Ag5PAAm-0.15x and 1Ag5PAAm-0.3x hydrogels is the crosslinker concentration (0.15 vs. 0.3 wt%). A subset of hydrogels was prepared only with 1wt% agarose (labeled as agarose hydrogels) as reference. The radius of the gels prepared in the petri dishes was 35 mm, while the thickness varied depending on the composition. After the gelation of the agarose and Ag-PAAm hydrogels in petri dishes, circular discs 2 mm in thickness and 8 mm in diameter were punched out and equilibrated either in DI water or in mixtures of DI water and dimethyl sulfoxide (DMSO) for one day prior to testing. We compare the results in this work with those reported for PAAm hydrogels in our previous works [33, 34]; note that the nomenclature has changed since we called the gels before 4%, 6% and 9% PAAm hydrogels, and now 4%, 5% and 8% PAAm hydrogels but the composition is the same. The 4%, 5% and 8% reflect only the acrylamide (monomer) concentration, while the crosslinker is given separately in the hydrogels' nomenclature to emphasize that various crosslinker concentrations have been selected for the same monomer concentration.

2.2 Attenuated Total Reflection Infrared Spectroscopy

Attenuated Total Reflectance Infrared Spectroscopy (ATR-IR) (PerkinElmer, Frontier, and Pike Technologies, GladiATR with a diamond crystal) was used to determine the chemical footprint of the DN hydrogels. The sample absorbance was collected in the range of 500–4000 cm^{-1}. The data are shown after baseline correction with DI water as background to enhance the polymer footprint. For infrared spectroscopy, hydrogel samples were prepared in the petri dishes, as described above, and the top and bottom surfaces were placed on the ATR-IR crystal to evaluate the presence of chemical gradients. Because the penetration depth of the infrared ranges between 1.1 and 2.2 µm, this is a viable method to distinguish between the relative concentrations of agarose and polyacrylamide close to top and bottom surfaces [35] and assess the presence of compositional gradients. A dead weight of ~ 100 g was placed on top of the hydrogels to enhance the hydrogel-crystal contact for each run.

2.3 Rheology

The rheological behavior of the hydrogels was investigated using a Dynamic Mechanical Analysis (DMA, Perkin Elmer, DMA 8000). Frequency and amplitude sweeps using the single cantilever mode were performed in the range of 0.1–20 Hz at constant strain of 2% and as a function of strain from 0.1 to 1% at a constant frequency of 1 Hz, respectively. Storage (G') and loss moduli (G'') were measured as a function of frequency and amplitude. For each measurement, the temperature was maintained constant at 25ºC using a water bath.

2.4 Swelling

Samples were weighed after 0, 4, 8, 12, 24 and 48 h immersion in the solvent. 48 h were long enough to achieve equilibrium swelling in the hydrogels. The swelling ratio was calculated as the weight of the swollen hydrogel over the as-prepared weight of the hydrogel.

2.5 Dynamic Light Scattering

Rectangular slabs were cut from hydrogel samples and inserted in a plastic cuvette. The cuvette was then filled with DI or mixtures of DI and DMSO to prevent hydrogel from drying. A Zetasizer 3000 (Malvern, USA) was used at a fixed wavelength λ of 632 nm and a scattering angle θ of 90°. For the analysis, we use the heterodyne approach by Joosten, McCarthy, and Pusey [36] for hydrogels, which considers the intrinsic heterodyne overlay of both the scattering from thermal dynamic concentration fluctuations and that from time-constant spatial concentration inhomogeneity. The method has been shown to work well when the inhomogeneities are not fully frozen inside the gel but display some residual slow mobility. Based on this approach, Tanaka's model is used to calculate an apparent diffusion coefficient D_{app} [37]as:

$$g^{(2)}(\tau) - 1 = \beta\sigma_I^2 \exp\left(-2D_{\text{app}}q^2\tau\right) \tag{1}$$

where $g^{(2)}(\tau)$ is the autocorrelation function (if the hydrogels are treated as ergodic media), β is the instrument coherence factor (assumed to be 1), σ_I^2 is the initial amplitude of the intensity autocorrelation function, q is the wave vector and τ is the correlation time. The ratio between the scattering from thermal dynamic concentration fluctuations $I_F(q)$ and the total scattering intensity $I(q)$ is given by:

$$X = \frac{< I_F(q) >_T}{< I(q) >_T} = 1 - \sqrt{1 - \sigma_I^2} \tag{2}$$

This yields following expressions for the collective diffusion coefficient D_c

$$D_c = (2 - X)D_{app} \tag{3}$$

and for the dynamic gel polymer network correlation length ξ_c

$$\xi_c = \frac{k_B T}{6\pi\eta D_c} \tag{4}$$

where η is the solvent viscosity, k_B is the Boltzmann constant, and T is the temperature. This method is adequate if the hydrogel inhomogeneities are not fully frozen inside the gel but display some residual slow mobility. For completely frozen inhomogeneities, more elaborated spatial-dependent DLS measurement and analysis are available [38], which are outside the scope of this work.

2.6 Colloidal Probe Atomic Force Microscopy

Indentation and friction force measurements were conducted with an atomic force microscope (AFM, Nanowizard Ultra, JPK Instruments, Germany) using silica colloids (Duke Scientific, Thermo Scientific, CA, USA) with nominal diameters of 20 µm. The colloids were attached to tipless cantilevers (spring constant k_n= 0.4 N/m, CSC37-No Al/tipless, Nanoandmore, USA) using an epoxy glue (JB-Weld, Sulphur Springs, TX, USA). The normal stiffness of the cantilevers was determined by the thermal noise method and the lateral stiffness was obtained by means of the wall calibration method [39]. For indentation and friction force measurements, the hydrogels were used as prepared in the petri dish. Indentation measurements were conducted at an approach/retraction velocity of 2 µm/s and an applied load of 20 nN.

The JKR model [40] was used to fit the retract curves via a least squared curve fitting algorithm built in MATLAB using the following equations:

$$h = h_c + \frac{a^2}{3R} + \frac{F}{2aE^*} \tag{5a}$$

$$a^3 = \frac{3R}{(4E^*)}(F + 3\pi\gamma + (6\pi\gamma RF + \left(3\pi\gamma R)^2\right)^{\frac{1}{2}}\Big) \tag{5b}$$

where F is the indentation force, h the indentation depth,h_c the contact point, R the colloid radius (determined from reverse imaging), a the contact radius, E^* the contact elastic modulus and γ the adhesion energy. Here, we have used the noise of the instrument (0.06 nN) as the baseline and defined the contact point at the tip position where the force exceeded 0.06 nN. The fits to the experimental data provide γ and E^* and thereby the elastic modulus of the hydrogels:

$$\frac{1}{E^*} = \frac{1 - v_1^2}{E_1} + \frac{1 - v_2^2}{E_2} \tag{6}$$

where E_1, v_1 (v_1 = 0.45 for the hydrogel) and E_2, v_2 (v_2 = 0.168 and E_2= 72.2 GPa)[41] are the elastic moduli and Poisson's ratio of the hydrogel and the silica colloid, respectively.

In addition to this, the Hertz contact model was fit to the approach curves in a piecewise manner, as described in detail in refs [33, 42], to extract elastic modulus as a function of indentation depth using the following equation:

$$F = \frac{4}{3}E^* R^{1/2} h^{3/2} \tag{7}$$

Note that this approach neglects viscoelastic and poroelastic effects on the resistance to indentation. However, the satisfactory agreement between the elastic moduli obtained from fits of Eq. (7) to indentation curves and from rheology supports the validity of this method.

Friction force measurements were performed at varying normal loads in the range 10–50 nN with sliding velocities spanning over almost three orders of magnitude in the range of 1–500 µm/s. At least 8 lateral force loops -each taken while the probe slid in forward (trace) and reverse (retrace) directions- were collected for each condition. The version of the JPK software used for data processing is 6.1.163. The friction force was calculated by averaging over the half width of the trace-retrace loops using a GUI developed in MATLAB.

2.7 Quantitative Imaging AFM

The hydrogel surfaces were imaged by AFM (Nano Wizard, JPK Instruments, Germany) using the quantitative imaging mode (QI) with a sharp tip (HQ:CSC37, No Al, 0.3–0.9 N m − 1, Nanoandmore, USA). In QI mode, cross-Sects. (30 × 30 µm and 5 × 5 µm) were divided into a grid of 256 × 256 pixels and force–distance curves were measured at each pixel at an approach speed of ~60 µm/s and a

very small load of ~1.5–2 nN. Maps of height, adhesion, and stiffness were obtained by QI.

3 Results

1Ag4PAAm-0.1x, 1Ag5PAAm-0.15x, 1Ag5PAAm-0.3x and 1Ag8PAAm-0.48x hydrogels were prepared as indicated in the Experimental section. Table 1 shows the composition of the prepared hydrogels, all of them with 1 wt% agarose as the first network and PAAm as the second network with AAm concentrations of 4, 5, 5 and 8 wt% for 1Ag4PAAm-0.1x, 1Ag5PAAm-0.15x, 1Ag5PAAm-0.3x, and 1Ag8PAAm-0.48x hydrogels, respectively. Note that 1Ag5PAAm-0.15x and 1Ag5PAAm-0.3x hydrogels were prepared with the half of the crosslinker concentration and the same monomer concentration.

3.1 Chemical Make-up of the Double Networks and Compositional Gradients

ATR-IR spectroscopy was used to identify the chemical footprint of bottom and top surfaces of the hydrogels. Figure 1 shows representative IR spectra for the four hydrogels. The successful polymerization of acrylamide in 1Ag4PAAm-0.1x hydrogels (Fig. 1A) is confirmed by the detection of strong absorption bands at 1672 cm^{-1} and 1599 cm^{-1} (dotted lines), -characteristic of amide I and amide II- on top and bottom surfaces. Additionally, the presence of the agarose is confirmed via the vibration bands at 1080 cm^{-1} for C–H bending in sugars, 1048 cm^{-1} for C–O, 1371 cm^{-1} for C–C bending, and 931 cm^{-1} ascribed to the 3,6-anhydrogalactose [43, 44]. Interestingly, broadened peaks at 1436 cm^{-1} and 1458 cm^{-1} are also observed in all IR spectra, which point toward the asymmetric stretching of COO- (blue solid lines). This can be due to the hydrolysis of AAm, expected to occur above 40 °C, [45] and is most prominent in the top and bottom surfaces of 1Ag4PAAm-0.1x hydrogels. Importantly, this hints towards the presence of charge, which could justify the highest swelling of this hydrogel (Figure S1).

The analysis of peak shifts corresponding to amide and C-O bands revealed two important findings. First, compared to the 1608 cm-1 amide II band for pure PAAm hydrogels (Figure S2), 1Ag8PAAm-0.48x showed a shift to lower wavenumbers, i.e., 1599 cm^{-1} and 1600 cm^{-1} for the top and bottom surfaces, respectively, while 1Ag5PAAm-0.3x showed a shift to 1600 cm^{-1} only for the top surface. A shift of this band to lower wavenumbers is commonly attributed to hydrogen bonding [23, 46]. In the case of the DN hydrogels, it could be associated with hydrogen bonding with agarose. For 1Ag4PAAm-0.1x and 1Ag5PAAm-0.15x, a shift to higher wavenumbers (1613 cm^{-1} and 1610 cm^{-1}, respectively) was observed for both top and bottom surfaces. This indicates that the intermolecular interactions between agarose and PAAm are weaker in these gels. Interestingly, the C-O peak in pure agarose hydrogels at 1046 cm^{-1} shifts to higher wavenumbers in the Ag-PAAm hydrogels, which supports that the formation of the second network reduces hydrogen bonding in agarose. Cooperative hydrogen bonding in agarose is crucial to form a thick fibrous network [47].

We also note that agarose and PAAm footprints, although detected on top and bottom surfaces of the four hydrogels, vary in intensity, pointing towards chemical gradients. (Figs. 1b–d). To evaluate the compositional gradients, Fig. 2 compares the ratios between the absorbance peaks at 1080 cm^{-1} (C–O) and at 1672 cm^{-1} (amide I) for top and bottom near-surface regions. The similar ratios for

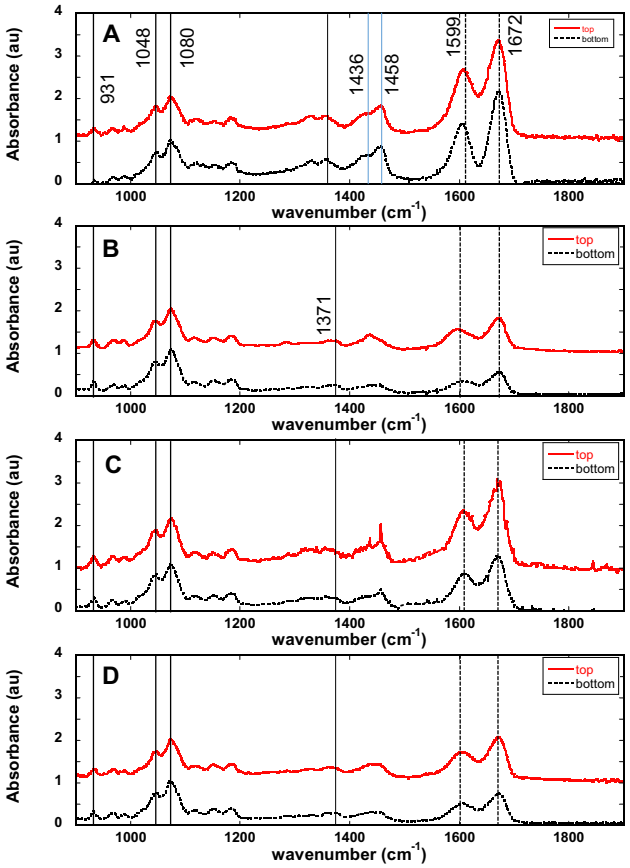

Fig. 1 ATR-IR absorbance spectra for **A** 1Ag4PAAm-0.1x–0.1x, **B** 1Ag5PAAm-0.3x, **C** 1Ag5PAAm-0.15x and **D** 1Ag8PAAm-0.48x hydrogels. Vibration bands associated with PAAm and agarose are identified as the dashed and full vertical lines, respectively (see text). The chemical heterogeneity of the hydrogels is illustrated by comparing between the IR spectra of top (red curves) and bottom (black curves) near-surface regions. The blue solid lines at 1436 and 1458 cm^{-1} highlight bands corresponding to the asymmetric stretching of COO-. For comparison, the vibration band for C–O in agarose single networks occurs at 1046 cm^{-1}, while the amide II band for polyacrylamide is located at 1608 cm^{-1} (Color figure online)

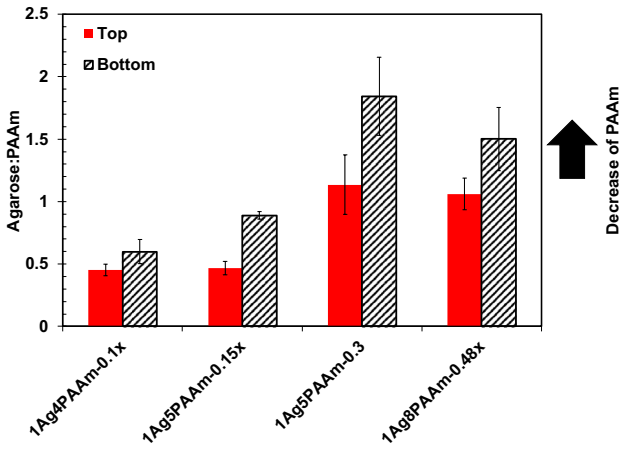

Fig. 2 Ratios between the absorbance at 1080 cm-1 (agarose peak) and at 1672 cm-1 (amide I peak) for top (red) and bottom (gray shadowed) near-surfaces regions of the four hydrogels (Color figure online)

1Ag4PAAm-0.1x indicate that the difference in composition of top and bottom surface regions is small. For the 1Ag5PAAm-0.15x hydrogel, Fig. 2 suggests an enrichment of acrylamide on the top compared to the bottom near-surface region. The gradient in composition is largest for 1Ag5PAAm-0.3x hydrogels. The increasing ratio indicates the depletion of PAAm toward the bottom near-surface region (in gray). Interestingly, increasing the acrylamide concentration to 8% at the same monomer-to-crosslinker ratio leads to a relative enrichment of PAAm in the bottom surface region, as evidenced by the decrease in absorbance ratio.

3.2 Composition-Dependent Strengthening, Adhesion, and Microstructural Gradients of Ag-PAAm Hydrogels

Based on amplitude sweeps (Figure S3), the hydrogels exhibit a prominent viscoelastic solid behavior, with a plateau storage modulus $G' < G''$ (the loss modulus), and tan-$\delta < 0.1$. Figure 3A shows G' and G'' of the hydrogels, as determined from amplitude sweeps at 1 Hz. The storage moduli are 17.1 ± 0.6 kPa, 109.4 ± 16.3 kPa, 13.7 ± 1.1 kPa, 9.7 ± 1 kPa for 1Ag4PAAm-0.1x, 1Ag5PAAm-0.15x, 1Ag5PAAm-0.3x and 1Ag8PAAm-0.48x hydrogels, respectively. In comparison, the storage modulus of agarose hydrogels (1 wt%) is 20.8 kPa±7.4, while the PAAm hydrogels with 4%, 5% and 8% PAAm have much smaller storage moduli: 0.143 kPa±0.01, 0.275 kPa±0.03, 1.14 kPa±0.15, respectively [34]; rheology measurements on 5%-0.15x PAAm (SN) hydrogels failed because the hydrogels were very soft. The comparison of results reveals that only 1Ag5PAAm-0.15x hydrogels led to significant strengthening: G' of 1Ag5PAAm-0.15x hydrogels is about one and three orders of magnitude larger than that of the SN agarose and PAAm hydrogels with similar monomer concentrations, respectively. Increasing the crosslinking concentration by a factor of two weakened the hydrogel significantly, as G' of 1Ag5PAAm-0.3x hydrogels decreased by one order of magnitude. 1Ag4PAAm-0.1x, 1Ag5PAAm-0.3x and 1Ag8PAAm-0.48x hydrogels have tan-δ values in the range 0.068–0.093 (-), like agarose hydrogels, while only 1Ag5PAAm-0.15x exhibit significantly smaller values [~ 0.028 (-)]. We note that, in contrast to the expected relation between polymer concentration and elastic modulus for SN hydrogels based on de Gennes scaling equations [48], we do not find a relation between storage modulus and the swelling ratio of the Ag-PAAm hydrogels; see swelling ratios in Fig. S1. Based on these rheology measurements, only 1Ag5PAAm-0.15x hydrogels can be classified as double network hydrogel since the other investigated compositions do not induce any strengthening compared to SN agarose hydrogels.

To characterize the dynamic correlation length of the Ag-PAAm networks, we used DLS. Figure S4 shows autocorrelation functions for the investigated hydrogels. 1Ag5PAAm-0.3x hydrogels exhibit fast and slow decay modes, which cannot be evaluated by the heterodyne approach (see Experimental methods), and hence, we do not discuss these results further. For the other hydrogels, a dynamic correlation length (ξ_c) can be determined, which represents the liquid-like concentration fluctuations of the polymer network. The fits to the correlation functions are shown in Figure S4 for representative measurements.

The correlation length for 1Ag4PAAm-0.1x, 1Ag5PAAm-0.15x, and 1Ag8PAAm-0.48x hydrogels is 90.6 ± 7.7 nm, 7.1 ± 0.1 nm and 135 ± 12 nm, respectively, while it is 10.1 ± 0.5 nm for agarose hydrogels (Fig. 3A, circles). An increase in mesh size occurs upon the addition of acrylamide (4% and 8%), while a noticeable decrease in mesh size is observed for 1Ag5PAAm-0.15x hydrogels. This correlation length reflects the intricate modulation of the polymer network via the second polymer. Importantly, the common scaling relation between mesh size and elastic modulus ($G' \sim \xi^{-3}$) for SN hydrogels [48]is not valid for these hydrogels.

The fit of the JKR model to the force-indentation curves upon retraction provides the work of adhesion γ. For agarose hydrogels, γ is small (0.024 ± 0.012 mN/m) and reflects the weak affinity of the hydrogel to the silica colloid. [49] This contrasts with the significant adhesion of 5% and 8% (SN) PAAm hydrogels (Fig. 3B, empty bars). The origin for this high adhesion has been associated with the formation of hydrogen bonds between PAAm and silanol groups [34]. The highest adhesion of 5% PAAm hydrogels results from the combined effects of a higher acrylamide concentration

than in 4% PAAm hydrogels and larger contact area than on 5%-0.15x and 8% PAAm hydrogels. Figure 3B shows that incorporating the PAAm network in the agarose hydrogel remarkably reduces the work of adhesion (patterned bars)– likely due to the presence of agarose on the hydrogel surface –, except in the case of 1Ag4PAAm-0.1x hydrogels. The latter is not surprising as both agarose and 4% PAAm hydrogels exhibit similar work of adhesion (~ 0.023 and 0.024 mN/m). The decrease in adhesion is most significant for 1Ag5PAAm-0.15x hydrogels, likely due to the concurrent strengthening of the hydrogel, which decreases the contact area.

The piecewise fit of the Hertz model to the force-indentation curves upon approach revealed a near-surface region (labeled as "skin") with a smaller Young's modulus than the hydrogel underneath (labeled as "bulk"); see Fig. 3C. The "skin" has a thickness of 146 ± 45 nm, 106 ± 25 nm, 305 ± 8.9 nm and 169 ± 47 nm with moduli of 1.6 ± 0.7 kPa, 12 ± 4.5 kPa, 0.6 ± 0.4 kPa, and 4.8 ± 0.9 kPa for the top surface of 1Ag4PAAm-0.1x, 1Ag5PAAm-0.15x, 1Ag5PAAm-0.3x and 1Ag8PAAm-0.48x hydrogels, respectively. While the existence of this skin is evident from the deviation of the resistance to indentation of the near surface region compared to the bulk hydrogel, the fits of the Hertz model cannot provide a precise quantification of the modulus of the skin. This is because the small thickness of this layer compared to the contact size breaks the condition of half-space body. Therefore, these values need to be considered with caution. The strongest hydrogel, 1Ag5PAAm-0.15x, has the thinnest skin layer, while the skin of 1Ag5PAAm-0.3x hydrogels is ~ 3 times thicker, softer, and depleted of PAAm (Fig. 2), but exhibits higher adhesion, likely due to the smaller modulus, and hence, larger contact area. This suggests that the reduction of the crosslinking density in 1Ag5PAAm-0.15x hydrogels enables the formation of a more uniform microstructure across the hydrogel depth. Underneath the skin, the highest Young's modulus is obtained for 1Ag5PAAm-0.15x hydrogels (80.5 ± 6.1 kPa), while similar moduli (19.9 ± 1.3 kPa, 10.8 ± 1.5 kPa and 13.9 ± 0.9 kPa) are obtained for 1Ag4PAAm-0.1x, 1Ag5PAAm-0.3x, and 1Ag8PAAm-0.48x hydrogels, respectively. These results are in qualitative agreement with the rheological results, and with the elastic modulus obtained using the JKR model.

3.3 Strengthening vs. Lubrication

The kinetic friction force between the hydrogels and a silica colloid as a function of load and velocity is shown in Fig. 4A–D. The measurements with 1Ag5PAAm-0.3x hydrogels were noisy and irreproducible, which we attribute to the presence of heterogeneities, and hence, they are not further discussed. The common trend for the other four hydrogels is that friction increases with load, while the velocity dependence of friction depends on the composition. Our previous investigations of the frictional characteristics of PAAm (SN) hydrogels revealed the existence of adhesive and viscous contributions to friction leading to a prominent decrease of friction with velocity (velocity-weakening friction) at slow sliding velocities and to an increase of friction with velocity (velocity-strengthening friction) at high velocities [34].

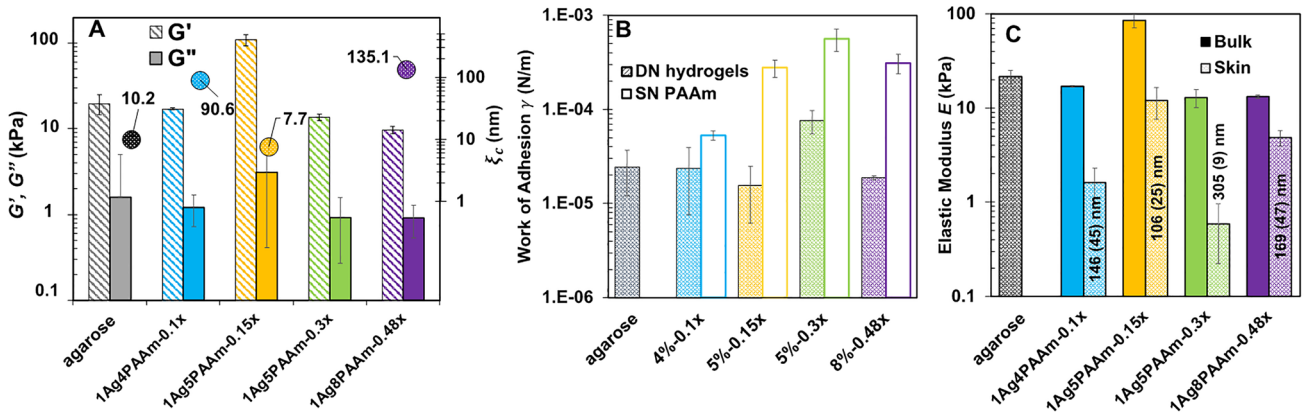

Fig. 3 Properties of agarose (1Ag, grey), 1Ag4PAAm-0.1x (blue), 1Ag5PAAm-0.15x (yellow), 1Ag5PAAm-0.3x (green), and 1Ag8PAAm-0.48x (purple) hydrogels. **A** Correlation lengths (circles) from DLS, as well as storage modulus (G', patterned bars) and loss modulus (G'', full bars) from strain amplitude sweeps. **B** Work of adhesion γ of agarose (grey patterned bar), Ag-PAAm (full bars) and PAAm (empty bars) hydrogels obtained from fitting the JKR model; the x-axis gives the acrylamide and bisacrylamide contents with either 0 wt% (SN hydrogels) or 1 wt% agarose (DN hydrogels), while agarose refers to agarose (SN) hydrogels. Work of adhesion for 4%, 5% and 8% PAAm hydrogels have been taken from ref. [34]. C Elastic modulus obtained from fits of the Hertz model to the AFM indentation results at two depths to determine the modulus of the "skin" (patterned bars) and of the hydrogel underneath (full bars). The thickness of the skin is given in the plot. Colloid radius for AFM experiments in **B** and **C**: 10 µm. Figure S5 shows representative force-indentation curves. Cantilever stiffness: 0.42 N/m (Color figure online)

Both the poroelastic drainage and the hydrogen bonding between acrylamide and the silica colloid led to a remarkable velocity-weakening friction. In contrast, a prominent velocity independent plateau at low velocities followed by an increase in friction with velocity at higher velocities is observed for agarose hydrogels (Fig. 4D).

The friction behavior of 1Ag4PAAm-0.1x hydrogels (Fig. 4A) resembles that of 4%PAAm (SN) hydrogels [34], with a prominent decrease in friction with velocity preceding a weak increase of friction with velocity. The friction loops exhibit an initial tilt before sliding commences, which is more prominent at slow velocities (Figure S6A), and it has been associated to the (time-dependent) poroelastic deformation of the surface-near region. [34, 50, 51] Furthermore, although subdued, the characteristic stick–slip can be associated with the interaction of PAAm with the silica colloid upon the drainage of water. Both phenomena can justify the prominent velocity-weakening friction.

In contrast, the frictional response of 1Ag5PAAm-0.15x and 1Ag8PAAm-0.48x hydrogels resembles the behavior of agarose hydrogels more closely, although they are less lubricious, especially 1Ag5PAAm-0.15x hydrogels. Both 1Ag5PAAm-0.15x and 1Ag8PAAm-0.48x hydrogels show a *quasi*-speed-independent plateau followed by velocity-strengthening friction, with the transition occurring at ~ 10 µm/s and 3–10 µm/s (increasing with increasing load), respectively. The absence of the velocity-weakening regime indicates that the poroelastic deformation is less significant. In the case of 1Ag5PAAm-0.15x hydrogels, the larger elastic modulus must reduce the contact area and the drainage of water. In the case of the much softer 1Ag8PAAm-0.48x hydrogels, the lack of the velocity-weakening regimes correlates with the smaller amount of PAAm in the near-surface region compared to 1Ag4PAAm-0.1x and 1Ag5PAAm-0.15x hydrogels, so that the frictional characteristics are mainly dictated by agarose. Note that significant stick–slip was observed for 1Ag5PAAm-0.15x hydrogels (Figure S6B, thereby supporting the interaction between PAAm and the colloid, whereas 1Ag8PAAm-0.48x (Figure S6C) shows smooth sliding, similar to that observed for agarose.

Friction coefficients (CoF) of the Ag-PAAm hydrogels ranged from $2.2.10^{-2}$ to 5.10^{-3} (Fig. 5), where the lowest and highest friction coefficients were recorded for 1Ag8PAAm-0.48x and 1Ag4PAAm-0.1x hydrogels, respectively; CoF was determined at ~ 0.1 µm/s to minimize hydrodynamic effects. The best lubrication is provided by agarose hydrogels (µ ~ 0.003 at 0.1 µm/s). The CoF obtained for 1Ag5PAAm-0.15x hydrogels is an improvement in comparison to the reported performance of some DN hydrogels [20, 29, 31]. The values of the CoF of the SN hydrogels were determined in our previous work (~ 0.05–0.077, see caption of Fig. 5) and are higher than the values reported here. With an increase in velocity, as viscous dissipation becomes gradually more relevant, the increase in friction is more prominent in the Ag-PAAm hydrogels compared to agarose hydrogels in water.

3.4 Tunable lubricious behavior of Ag-PAAm hydrogels via the imbibed fluid

Mixtures of DMSO and water were used to modulate the viscosity of the imbibed fluid in agarose and 1Ag5PAAm-0.15x hydrogels and examine its influence on the swelling ratio, colloidal probe indentation, surface topography and frictional characteristics of the gels. The change of the swelling ratio of 1Ag5PAAm-0.15x hydrogels is moderate, with a decrease from 173 to 160% with addition of 50% DMSO and to 132% in pure DMSO. In comparison, the swelling ratio of agarose decreases from ~ 193% in DI water, to 104% and 61% in 50% and 100% DMSO, respectively, and hence, there is a more significant collapse of the agarose hydrogels. The elastic modulus of the hydrogels obtained by colloidal probe indentation is 100 ± 5.3, 62.7 ± 3.58 and 52.2 ± 9.2 kPa for 1Ag5PAAm-0.15x hydrogels in 0%, 50% and 100% DMSO, and 21.58 ± 3.58, 9.8 ± 2.73 and 5.44 ± 0.5 kPa for agarose hydrogels in 0%, 50% and 100% DMSO, respectively. The work of adhesion is 0.0244, 0.872 and 0.185 mN/m for agarose hydrogels in 0%, 50% and 100% DMSO, whereas the

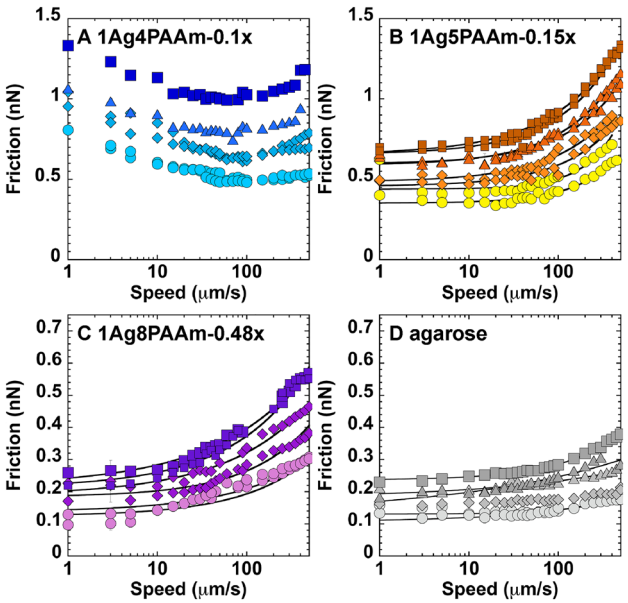

Fig. 4 Friction force vs. sliding speed for **A** 1Ag4PAAm-0.1x (blue), **B** 1Ag5PAAm-0.15x (yellow to orange), **C** 1Ag8PAAm-0.48x (purple) and **D** agarose (grey) hydrogels at normal loads of 20 nN (circles), 30 nN (diamonds), 40 nN (triangles) and 50 nN (squares). The solid black lines in B-D are fits of Eq. 1 to the experimental results. Colloid radius: 10 μm. Cantilever Stiffness: 0.42 N/m (Color figure online)

work of adhesion of 1Ag5PAAm-0.15x hydrogels vanishes upon addition of DMSO. We thus observe a decrease in the elastic modulus of both types of hydrogels, which is consistent with a smaller osmotic pressure and modulus. The change of the swelling behavior of agarose hydrogel must be related to the reduction of the ability of agarose to form crystalline junctions (crosslinkers) in DMSO-water mixtures [52]. In addition, DMSO is a bad solvent for polyacrylamide at room temperature [53], which should cause a collapse of polyacrylamide gels in this solvent. However, the moderate collapse of the DN hydrogels suggests that the double network hinders the overall collapse.

The DN hydrogel's surface in 50% DMSO (Fig. 6D–F) is stiffer and less adhesive, and shows circular domains, ranging in diameter from ~ 4.5 to 5.7 µm. In contrast, the surface structure is uniform in water (Fig. 6A–C) and 100% DMSO (Figure S8). The depth of these cavities ranges from 300 to 500 nm. More prominent circular domains are observed when the synthesis of the DN hydrogel is conducted directly in 50% DMSO (Fig. 6G–I). The observed circular domains may thus reflect the heterogeneous collapse of the hydrogels, at least near the surface, likely in regions where PAAm is enriched. We note that 50% DMSO in water is used for the synthesis of macroporous PAAm hydrogels below 0ºC, as the solvation-induced phase separation due to the high affinity between water and DMSO[54, 55] causes a porous structure to form [56, 57]. Based on this, the observed circular domains could result from a local phase separation and collapse of PAAm. However, our sample preparation and measurements were conducted at room temperature, and hence, this is only a speculation at this point. Reference images of SN agarose hydrogel in 50% DMSO are shown in Figure S9.

Figure 7 shows friction measurements in 0%, 50% and 100% DMSO for agarose and 1Ag5PAAm-0.15x hydrogels. The friction force between the colloid and agarose hydrogels decreases upon addition of DMSO at slow velocity, while it increases at high velocity, with the highest friction measured in 100% DMSO (Fig. 7A–C), which is concurrent with the increase in viscosity; note that the viscosity of water, 50% DMSO and 100% DMSO is 1, 2.83 and 1.99 mPa.s at 25ºC, respectively [58]. In the case of 1Ag5PAAm-0.15x hydrogels, an increase in DMSO concentration to 50%, however, provides better lubrication than in water (Fig. 7D–E), and there is a further improvement in lubrication in 100% DMSO (Fig. 7F), also at high velocities and despite the increase in viscosity. Here, the more significant volume fraction of imbibed fluid in the DN hydrogel compared to agarose in pure DMSO (see swelling ratios) correlates with the more lubricious behavior. However, we are aware that the swelling behavior of a hydrogel is a bulk property, whereas the frictional characteristics are significantly influenced by the properties of the near-surface region, and hence, caution should be taken with this comparison. Because the frictional response is related to

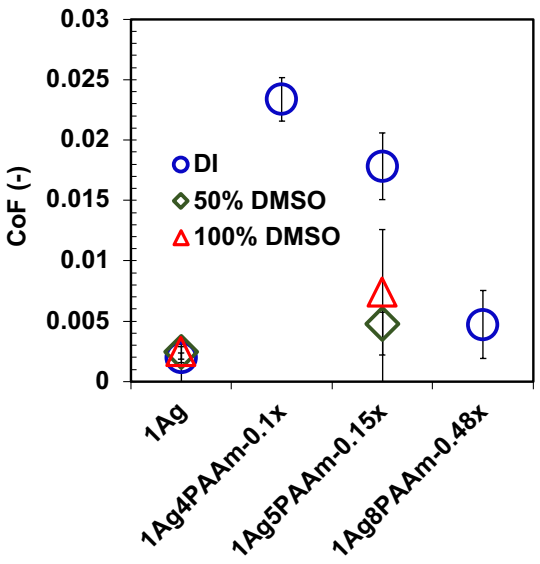

Fig. 5 Coefficient of friction for agarose, 1Ag4PAAm-0.1x, 1Ag5PAAm-0.15x and 1Ag8PAAm-0.48x hydrogels in DI water (blue circles), 50% DMSO (green diamonds) and 100% DMSO (red squares) at a sliding velocity of 0.1 µm/s. The three values superpose in the case of agarose hydrogels. The CoF for 4PAAm-0.1x, 5PAAm-0.3x and 8PAAm-0.48x hydrogels (SN) is 0.067, 0.050 and 0.077 (-), respectively[34]. The friction measurements for 5PAAm-0.15x failed repeatedly likely due to the softness of these hydrogels (Color figure online)

the topography of the near-surface region also in the case of hydrogels [59], the circular domains are also expected to influence the frictional characteristics of the hydrogel.

Based on the adhesive-viscous model for hydrogel lubrication [34], the viscous component of friction is described based on the Couette flow of a fluid film composed of polymer and fluid:

$$F_{vis} = F_0 + \eta_{eff} V \bullet \Omega \tag{8}$$

where F_o is taken as a constant to describe the quasi-independent friction at slow velocities, $\Omega = \frac{16\pi}{5} R \log\left(\frac{2R}{d}\right)$ is a geometric constant, R is the colloid radius, $\eta_{eff} \sim \eta_0 (V/d)^n$ with $n < 0$ (for shear-thinning behavior) and d is the thickness of the sheared film, which is assumed to be equal to the hydrogel's dynamic correlation length [60]. Hence, we took d to be ξ_c=10.2, 7.7 and 135 nm, for agarose, 1Ag6PAAm-0.15x and 1Ag8PAAm-0.48x hydrogels, respectively (Fig. 3A). Admittedly, this is a simplification because the correlation length is a bulk property and the near-surface region could exhibit a different correlation length due to the varying crosslinking degree.

The lines in Fig. 4 and 7 show the fits of Eq. 8 to the experimental results. The good fit of the model to the friction force between the silica colloid and hydrogels points towards a hydrodynamic lubrication owing to the

low adhesion at the contact. Figure 8A shows the viscosity parameter η_0 as a function of normal load, while the shear thinning exponent n is ~ − 0.32 for agarose and -0.39 for the two Ag-PAAm hydrogels. In agreement with our prior work on SN hydrogels, the increasing η_0 with load (between 20 and 50 nN) is evident for the three hydrogels and reflects the gradually greater influence of the polymer network on the viscous dissipation due to fluid exudation. This supports that both the polymer and the fluid influence the frictional dissipation based on this model. The highest viscosity parameters in water (η_0~0.2 to 0.33) are observed for 1Ag5PAAm-0.15x hydrogels, while the smallest viscosity parameters (η_0~0.01 to 0.03) are obtained for the agarose hydrogels, reflecting the weaker increase of friction with velocity. We note that the higher viscosity parameter of 1Ag5PAAm-0.15x hydrogels in water cannot be explained by the bulk swelling ratio, which is similar for the three hydrogels. Both η_0 and n must be significantly affected by the properties of the skin layer. We note that 1Ag8PAAm-0.48x hydrogels have a thick and soft skin layer, possibly arising from the disturbed crosslinking of agarose, which results in a weak and loose network with depleted PAAm. This is in contrast with the thinner and stiffer skin layer of 1Ag5PAAm-0.15x hydrogels, yielding a higher viscosity parameter.

Figure 8B–C shows that the viscosity parameter of agarose and 1Ag5PAAm-0.15x hydrogels changes with DMSO%. For both hydrogels, the value of η_0 exhibits a maximum at 50% DMSO, which is consistent with the maximum viscosity of water-DMSO mixtures and reflects the role of the solvent in lubrication, except at a load of 50 nN on agarose hydrogels. However, note that the evolution of the shear thinning exponent is quite different for both hydrogels: n increases from − 0.32 to ~ − 0.24 for agarose hydrogels, whereas the opposite behavior is observed for the 1Ag5PAAm-0.15x hydrogels, as n decreases from -0.39 to ~ − 0.48. This indicates that despite the non-adhesive nature of the contacts (see small work of adhesion compared to PAAm hydrogels, Fig. 3C), the polymer network influences lubrication and does it in a different manner in both hydrogels. The prominent collapse of agarose hydrogels in DMSO mixtures is concurrent with the less significant shear

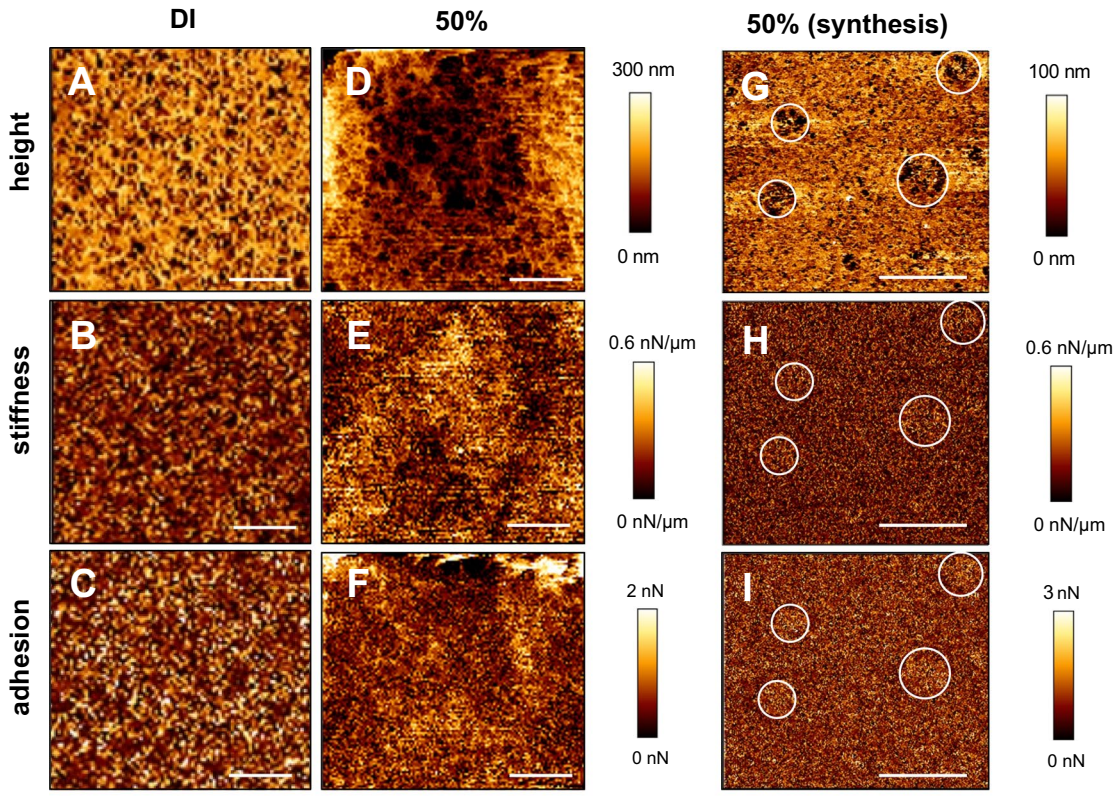

Fig. 6 QI images of the DN hydrogels equilibrated in **A**–**C** DI (4×4 μm), **D**–**F** 50% DMSO (4×4 μm) and **G**–**I** synthesized in 50% DMSO (30×30 μm). Maps of **A**; **D**; **G** height, **B**; **E**; **H** stiffness and **C**; **F**; **I** adhesion for each condition. Increase in the color brightness points to an increase in height, stiffness or adhesion. Figure S7 shows the histograms of the surface stiffness and adhesion of the three hydrogels. The roughly circular region in 50% DMSO observed throughout the sample (see white circles to guide the eye), vary in size, with sizes ranging from 4.5 μm for the smallest and 5.7 μm for the largest observed features. The scale bars in A-F corresponds to 1 μm while in G-I they represent 10 μm. Tip: Si tip, stiffness: 0.37 N/m

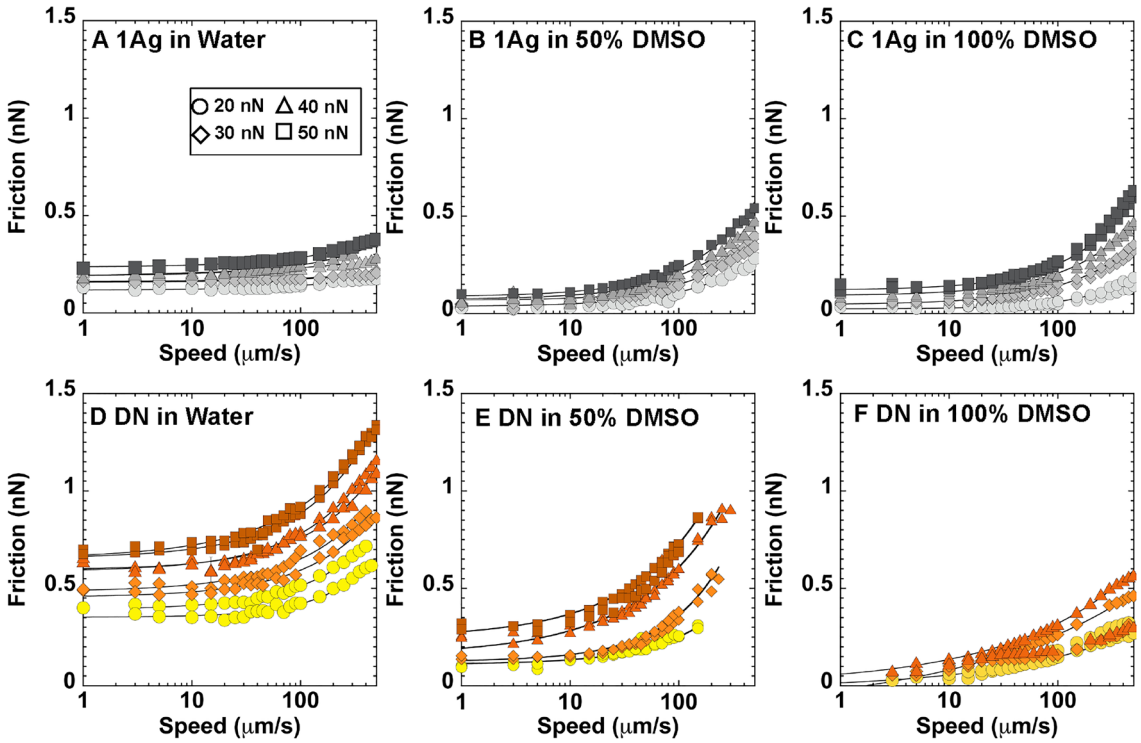

Fig. 7 Friction force as a function of sliding speed for agarose hydrogel in **A** 0% (DI), **B** 50% and **C** 100% DMSO, and 1Ag5PAAm-0.15x hydrogel in **D** 0% (DI), **E** 50% and **F** 100% DMSO. Results are shown for four different normal loads: 20 nN (circles), 30 nN (diamonds), 40 nN (triangles) and 50 nN (squares). Colloid diameter: 10 μm. Cantilever Stiffness: 0.42 N/m

thinning behavior. Although speculative at this point, we propose that a hydrogel or skin collapse reduces the effect of the polymer on lubrication owing to the polymer depletion and the solvent enrichment in the sheared interface. The more subtle decrease of the swelling ratio of 1Ag5PAAm-0.15x in 50% and 100% DMSO would thus reduce the influence of the polymer network less significantly. Furthermore, the heterogeneous structure might also play a role here. Hence, the response seems to be binary, where both the solvent viscosity and the response of the polymer network at the surface modulate the friction force.

4 Discussion

The results discussed in the previous section demonstrate the remarkable influence of small compositional variations of Ag-PAAm hydrogels on their microstructure, mechanical and tribological properties (Fig. 9A). Furthermore, the lubrication performance of the four Ag-PAAm hydrogels was not only quite different, but also responsive to the DMSO concentration. These results let us propose a pathway for the gelation of the investigated Ag-PAAm hydrogels that can justify the observed microstructures, different extents of strengthening and distinct lubrication performance.

The pre-polymer solution (AAm and bis-AAm) was added to the dissolved agarose solution at high temperature (~ 80 ° C). As the solution cooled down, the gelation of agarose started to form the first network. The gelation of agarose has been proposed to proceed by liquid phase separation of rod-like, helical segments in agarose polymer chains [61], forming a coacervate phase and a dilute phase. At the gelation point, the polymer in the dilute solution phase acts as an inter-coacervate junction. The coacervate particles are thus connected three-dimensionally, and the solution loses its fluidity to form a gel. The polymerization of the second network was initiated 30 min after cooling started, before the agarose network was completely formed [62]. A recent work by Gombert et al. [63] has revealed that the difference between the polymerization kinetics of bis-acrylamide and acrylamide leads to a hierarchical structure in PAAm hydrogels. Briefly, bis-AAm-rich areas polymerize first in the solution and are not connected in the early polymerization phase (pre-gel phase). AAm molecules become incorporated in the bis-AAm-rich polymer clusters during the pre-gel reaction. While they also form polymer chains during this first polymerization stage, these chains are too short to connect the cross-linking clusters. AAm monomers polymerize into longer chains only after approximately 50% of all monomer in the reaction solution has reacted and a

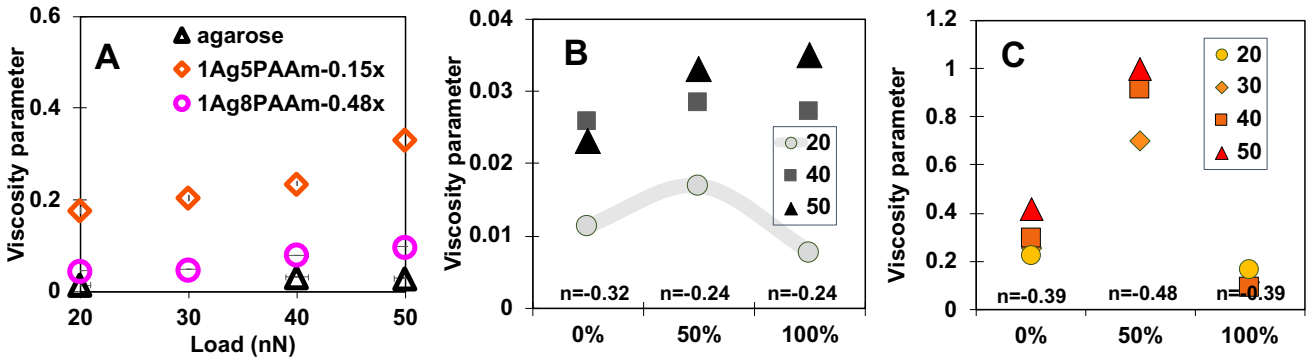

Fig. 8 Viscosity parameter η_0 for **A** agarose (black triangles), 1Ag5PAAm-0.15x (orange diamonds) and 1Ag8PAAm-0.48x (magenta circles) hydrogels in DI water with shear thinning exponents -0.32, -0.39 and -0.39, respectively, **B** agarose and **C** 1Ag5PAAm-0.15x hydrogels in water-DMSO mixtures. Translucent lines have been added to guide the eye (Color figure online)

significant fraction of the bis-AAm has polymerized. In this second phase of polymerization, AAm-rich polymer chains grow and connect the insoluble cross-linking clusters. For 7.5 wt% of AAm, and 0.1–0.48 wt%, Gombert et al. found that the smallest structure consists of clusters smaller than 4 nm in size, which agglomerate into domains that can grow to hundreds of nm and μm with increasing bis-acrylamide concentration [63]. For example, for 0.3 wt% bis-AAm that previous work observed clusters of 100 s nm in size interconnected by short polymer chains.

In our system, it is reasonable to expect that the crosslinker-rich clusters become confined in the dilute regions of agarose and voids, yielding important concentration fluctuations. While we do not know if the agarose network could prevent the clusters to grow to the same size as in pure solution, the larger dynamic correlation lengths ξ_c of 1Ag4PAAm-0.1x and 1Ag-8PAAm-0.48x suggest that the agarose network is influenced by the polymerization of the second network hydrogel. To form a double network, polyacrylamide chains need to be sufficiently large to connect the clusters in separate voids during the gelation phase. This can only happens if the crosslinker concentration is sufficiently small. Importantly, de Gennes addressed the problem of two chemically different, and hence weakly compatible polymers when crosslinked together [64], and found that higher crosslinking counteracted segregation, i.e. it extended the miscibility region. For our system, FTIR measurements support the weak interactions between acrylamide and agarose, and hence, there is no crosslinking between the two polymers. Therefore, the formation of a hydrogel microstructure via the segregation of the two polymers is not excluded.

The proposed pathway for the formation of the gels is thus represented in Fig. 9B. The competition between polymer segregation and the simultaneous polymerization of acrylamide and bis-acrylamide results in multiple network morphologies depending on the composition. If the polymer chains linking the clusters are too short, the interconnection of the second network across the agarose network will be poor and a double network will not form. This is more likely to happen at the highest crosslinking concentrations, i.e. in 1Ag5PAAm-0.3x and 1Ag8PAAm-0.48x hydrogels. The negligible strengthening of these hydrogels is consistent with the existence of a poorly interconnected second network across to the agarose hydrogels. By decreasing the crosslinker concentration (1Ag5PAAm-0.15x), the polymerization kinetics of bis-AAm slow down, the clusters decrease in size and the cross-linking efficiency and 2nd network increases, yielding yield longer PAAm chains that penetrate *across* the first network (one of the requirements of an effective DN gel), resulting in the enhancement of the mechanical properties (Fig. 9A). A similar mechanism was proposed for PAMPS/PAAm DN hydrogels. [65] It is interesting that the subtle decrease of AAm and bis-AAm concentration in 1Ag4PAAm-0.1x hydrogels leads to a significant increase in swelling ratio (and dynamic correlation length) and weakening compared to 1Ag5PAAm-0.15x . The results suggest that the second network is loose and can freely slide through the first network 1Ag4PAAm-0.1x hydrogels. Based on this discussion, a double network is only achieved for 1Ag5PAAm-0.15x hydrogels.

The influence of the different microstructures on the lubricious behavior of the hydrogels is also significant. First, the agarose network is able to reduce significantly the adhesion of PAAm to the countersurface, the silica colloid. It is also evident that the strongest hydrogels (1Ag5PAAm-0.15x) are not the most lubricious in water. Significant entanglements between the interpenetrating networks and/or crosslinking within the PAAm rich regions could hinder the facile motion of the polymers upon shear, yielding an increase in CoF. For the poorly interconnected 1Ag8PAAm-0.48x hydrogels, the shear of the second network would be further facilitated, justifying the decrease of the frictional dissipation. Nevertheless, the tribological performance of 1Ag8PAAm-0.48x and of 1Ag4PAAm-0.1x hydrogels seems

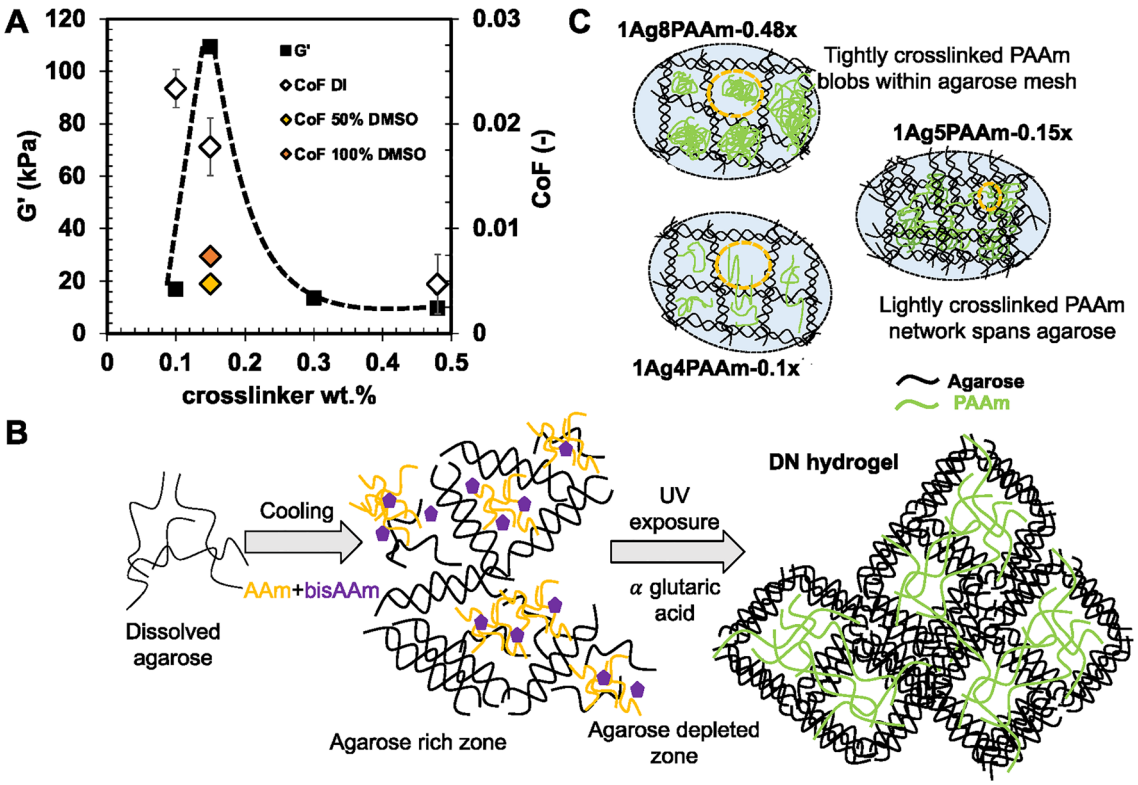

Fig. 9 **A** Storage modulus (black squares) obtained from rheological measurements as a function of the crosslinker concentration in the second network and the CoF measured on the Ag-PAAm hydrogels in DI (open diamonds), 50% DMSO (yellow diamonds) and 100% DMSO (orange diamonds). The dashed lines provide a guide to the eye. The different morphologies expected for the four hydrogel compositions are also shown. **B** Formation of Ag-PAAm hydrogels, starting with the agarose polymer, addition of Aam and bis-Aam and subsequent UV exposure: The agarose fibers undergo a coil to helix transformation and the helices further aggregate into thicker fibers which build the agarose hydrogel's network [47]. The voids are filled with the second network, which should be interpenetrating and crosslinked to achieve strengthening. This is achieved in this work only for 1Ag5PAAm-0.15x hydrogels. **C** Schematic map describing the various microstructures that can form depending on composition (Color figure online)

to be significantly affected by the content of PAAm in the near-surface region.

There is significant interest in modulating the frictional characteristics of hydrogels. Note that studies in SN hydrogels have shown the tunability of friction with water content (mesh size) [66], monomer/crosslinker concentration [33, 34, 67], solvent viscosity [68], as well as solvent quality with mixtures of ethanol–water [69]. Here, we have also demonstrated that varying the imbibed fluid can improve the lubrication performance of these hydrogels. This may be caused in part because the swelling behavior of the DN hydrogels is less responsive to the solvent quality of the DMSO-water mixtures compared to the parent SN hydrogels. This characteristic affords a higher range of fluids to be used as solvents of DN hydrogels. Furthermore, the response of friction to the solvent composition announces a novel strategy to modulate friction and lubrication via the imbibed fluid in DN hydrogels.

The work described here shows that a fine balance of composition is essential to render high strength to the hydrogel, which is consistent with Gong's initial findings about the formation of an efficient double network. Note that in our study, the concentration of agarose was kept constant. In a previous work, an approximately linear increase in the strength and toughness of Ag-PAAm hydrogels was obtained with agarose concentration above a critical value [70]. A maximum in strength or an upper critical concentration for achieving high strength was not mentioned, though. Based on our own results, the agarose network is sensitive to the PAAm concentration, and hence, the findings in this previous work may not be extrapolated to other PAAm concentrations in the double network.

While DN hydrogels can successfully overcome the challenge of enhanced mechanical properties via proper design, it is imperative that other functionalities, such as self-healing, electrical conductivity, injectability or tunable friction and adhesion are coupled with high strength. We have demonstrated that, with adequate choice of the first and second network, and of the imbibed fluid, we can concurrently achieve low friction and high strength. The results

shown here herald potential applications of DN hydrogels as advanced functional materials as replacement of biological tribosystems like the cartilage and for soft robotics.

5 Conclusion

The microstructure, mechanical and tribological response of Ag-PAAm hydrogels were studied by varying the second network's composition and the imbibing fluid. A nonlinear change of the mechanical properties was obtained as a function of varying PAAm composition, and a significant strengthening was only achieved by 1Ag5PAAm-0.15x hydrogels. A further increase in either the monomer concentration or in the crosslinking density, or both, lead to a loss of this enhancement. A mechanistic approach was proposed to understand the formation of an effective double network in this system. Additionally, friction measurements on the Ag-PAAm hydrogels revealed behaviors reminiscent of one of the two reference polymers, depending on which one enriched the surface. Apart from the hydrogels with the lowest monomer and crosslinker (4%PAAm), all other hydrogels showed a quasi-speed independent plateau, followed by viscous dissipation and shear thinning, in stark contrast to PAAm (SN) hydrogels. Modulation in friction by changing the imbibed fluid revealed a robust tribological response of the DN hydrogel in comparison to agarose (SN) hydrogels. The findings described here issue insights into the microstructure to property relationships of Ag-PAAm hydrogels and provide design perspectives to tune the mechanical and tribological response of these materials.

6 Supporting Information

Swelling ratios of Agarose-PAAm DN hydrogels, IR spectrum of PAAm, amplitude sweeps (G' and G'') from rheology, autocorrelation functions obtained from dynamic light scattering and friction loops for the double network hydrogels, quantitative imaging of 1Ag5PAAm-0.15x in 100% DMSO as well as of a single network agarose hydrogel in 50% DMSO.

Supplementary Information The online version contains supplementary material available at https://doi.org/10.1007/s11249-022-01604-4.

Acknowledgements We acknowledge the Materials Research Laboratory (MRL) at UIUC for providing the DLS facility.

Author Contributions All authors contributed to the study conception and design. Material preparation and data collection were performed by Tooba Shoaib and Paige Prendergast, and analysis was carried out by all authors. The first draft of the manuscript was written by Tooba Shoaib and all authors commented on previous versions of the manuscript. All authors read and approved the final manuscript.

Funding This material is based upon work supported by the National Science Foundation under Grant No. CMMI-1761696.

Declarations

Conflict of interest The authors have no relevant financial or non-financial interests to disclose.

References

1. Zhang, Y.S., Khademhosseini, A.: Advances in engineering hydrogels. Science (2017). https://doi.org/10.1126/science.aaf3627
2. Hoffman, A.S.: Hydrogels for biomedical applications. Adv. Drug Deliv. Rev. **64**, 18–23 (2012)
3. Brand, R.A.: Joint contact stress: a reasonable surrogate for biological processes? Iowa Orthop. J. **25**, 82–94 (2005)
4. Gong, J.P., Katsuyama, Y., Kurokawa, T., Osada, Y.: Double-network hydrogels with extremely high mechanical strength. Adv. Mater. **15**, 1155–1158 (2003)
5. Wang, M.X., Yang, C.H., Liu, Z.Q., Zhou, J., Xu, F., Suo, Z., et al.: Tough photoluminescent hydrogels doped with lanthanide. Macromol. Rapid Commun. **36**, 465–471 (2015)
6. Lake, G.J., Thomas, A.G.: The strength of highly elastic materials. Proc. R. Soc. Lond. A **300**, 108–119 (1967)
7. Sun, J.Y., Zhao, X., Illeperuma, W.R., Chaudhuri, O., Oh, K.H., Mooney, D.J., et al.: Highly stretchable and tough hydrogels. Nature **489**, 133–136 (2012)
8. Xu, X., Jerca, V.V., Hoogenboom, R.: Bioinspired double network hydrogels: from covalent double network hydrogels via hybrid double network hydrogels to physical double network hydrogels. Mater. Horiz. **8**, 1173–1188 (2021)
9. Haque, M.A., Kurokawa, T., Gong, J.P.: Super tough double network hydrogels and their application as biomaterials. Polymer **53**, 1805–1822 (2012)
10. Gao, G., Du, G., Sun, Y., Fu, J.: Self-healable, tough, and ultrastretchable nanocomposite hydrogels based on reversible polyacrylamide/montmorillonite adsorption. ACS Appl. Mater. Interfaces **7**, 5029–5037 (2015)
11. Lin, S., Cao, C., Wang, Q., Gonzalez, M., Dolbow, J.E., Zhao, X.: Design of stiff, tough and stretchy hydrogel composites via nanoscale hybrid crosslinking and macroscale fiber reinforcement. Soft Matter **10**, 7519–7527 (2014)
12. Ekblad, T., Bergstrom, G., Ederth, T., Conlan, S.L., Mutton, R., Clare, A.S., et al.: Poly(ethylene glycol)-containing hydrogel surfaces for antifouling applications in marine and freshwater environments. Biomacromolecules **9**, 2775–2783 (2008)
13. Tsukeshiba, H., Huang, M., Na, Y.H., Kurokawa, T., Kuwabara, R., Tanaka, Y., et al.: Effect of polymer entanglement on the toughening of double network hydrogels. J. Phys. Chem. B **109**, 16304–16309 (2005)
14. Nakajima, T., Furukawa, H., Tanaka, Y., Kurokawa, T., Osada, Y., Gong, J.P.: True chemical structure of double network hydrogels. Macromolecules **42**, 2184–2189 (2009)
15. Es-haghi, S.S., Leonov, A.I., Weiss, R.A.: On the necking phenomenon in pseudo-semi-interpenetrating double-network hydrogels. Macromolecules **46**, 6203–6208 (2013)
16. Arakaki, K., Kitamura, N., Fujiki, H., Kurokawa, T., Iwamoto, M., Ueno, M., et al.: Artificial cartilage made from a novel

double-network hydrogel: in vivo effects on the normal cartilage and ex vivo evaluation of the friction property. J. Biomed. Mater. Res. A **93**, 1160–1168 (2010)
17. Gu, Z., Huang, K., Luo, Y., Zhang, L., Kuang, T., Chen, Z., et al.: Double network hydrogel for tissue engineering. Wiley Interdiscip. Rev. Nanomed. Nanobiotechnol. **10**, e1520 (2018)
18. Nakajima, T., Gong, J.P.: Double-Network Hydrogels: Soft and Tough IPN, pp. 1–6. Springer, Berlin, Heidelberg (2013)
19. Chen, Q., Zhu, L., Huang, L., Chen, H., Xu, K., Tan, Y., et al.: Fracture of the physically cross-linked first network in hybrid double network hydrogels. Macromolecules **47**, 2140–2148 (2014)
20. Shi, Y., Li, J., Xiong, D., Li, L., Liu, Q.: Mechanical and tribological behaviors of PVA/PAAm double network hydrogels under varied strains as cartilage replacement. J. Appl. Polym. Sci. **138**, 50226 (2020)
21. Chen, Q., Zhu, L., Chen, H., Yan, H., Huang, L., Yang, J., et al.: A novel design strategy for fully physically linked double network hydrogels with tough, fatigue resistant, and self-healing properties. Adv. Func. Mater. **25**, 1598–1607 (2015)
22. Lin, T., Bai, Q., Peng, J., Xu, L., Li, J., Zhai, M.: One-step radiation synthesis of agarose/polyacrylamide double-network hydrogel with extremely excellent mechanical properties. Carbohydr. Polym. **200**, 72–81 (2018)
23. Cho, M.K., Singu, B.S., Na, Y.H., Yoon, K.R.: Fabrication and characterization of double-network agarose/polyacrylamide nanofibers by electrospinning. J. Appl. Polym. Sci. **133**, 42914 (2016)
24. Zhang, Y., Zhou, S., Zhang, L., Yan, Q., Mao, L., Wu, Y., et al.: Pre-Stretched double network polymer films based on agarose and polyacrylamide with sensitive humidity-responsive deformation, shape memory, and self-healing properties. Macromol. Chem. Phys. **221**, 1900518 (2020)
25. Mredha, M.T.I., Kitamura, N., Nonoyama, T., Wada, S., Goto, K., Zhang, X., et al.: Anisotropic tough double network hydrogel from fish collagen and its spontaneous in vivo bonding to bone. Biomaterials **132**, 85–95 (2017)
26. Yasuda, K., Kitamura, N., Gong, J.P., Arakaki, K., Kwon, H.J., Onodera, S., et al.: A novel double-network hydrogel induces spontaneous articular cartilage regeneration in vivo in a large osteochondral defect. Macromol. Biosci. **9**, 307–316 (2009)
27. Li, X., Wu, C., Yang, Q., Long, S., Wu, C.: Low-velocity superlubrication of sodium-alginate/polyacrylamide ionic-covalent hybrid double-network hydrogels. Soft Matter **11**, 3022–3033 (2015)
28. Yu, F., Cui, T., Yang, C., Dai, X., Ma, J.: kappa-Carrageenan/Sodium alginate double-network hydrogel with enhanced mechanical properties, anti-swelling, and adsorption capacity. Chemosphere **237**, 124417 (2019)
29. Kaneko, D., Tada, T., Kurokawa, T., Gong, J.P., Osada, Y.: Mechanically strong hydrogels with ultra-low frictional coefficients. Adv. Mater. **17**, 535–538 (2005)
30. Katta, J.K., Marcolongo, M., Lowman, A., Mansmann, K.A.: Friction and wear behavior of poly(vinyl alcohol)/poly(vinyl pyrrolidone) hydrogels for articular cartilage replacement. J. Biomed. Mater. Res. A **83**, 471–479 (2007)
31. Zhang, K., Simic, R., Yan, W., Spencer, N.D.: Creating an interface: rendering a double-network hydrogel lubricious via spontaneous delamination. ACS Appl. Mater. Interfaces **11**, 25427–25435 (2019)
32. Bonyadi, S.Z., Demott, C.J., Grunlan, M.A., Dunn, A.C.: Cartilage-like tribological performance of charged double network hydrogels. J. Mech. Behav. Biomed. Mater. **114**, 104202 (2021)
33. Shoaib, T., Espinosa-Marzal, R.M.: Influence of loading conditions and temperature on static friction and contact aging of hydrogels with modulated microstructures. ACS Appl. Mater. Interfaces **11**, 42722–42733 (2019)
34. Shoaib, T., Espinosa-Marzal, R.M.: Insight into the viscous and adhesive contributions to hydrogel friction. Tribol. Lett. **66**, 96 (2018)
35. Shoaib, T., Yuh, C., Wimmer, M.A., Schmid, T.M., Espinosa-Marzal, R.M.: Nanoscale insight into the degradation mechanisms of the cartilage articulating surface preceding OA. Biomater. Sci. **8**, 3944–3955 (2020)
36. Joosten, J.G.H., McCarthy, J.L., Pusey, P.N.: Dynamic and static light scattering by aqueous polyacrylamide gels. Macromolecules **24**, 6690–6699 (2002)
37. Siegert, A.J.F.: On the fluctuations in signals returned by many independently moving scatterers. Radiation Laboratory, Massachusetts Institute of Technology, Cambridge, MA (1943)
38. Seiffert, S.: Scattering perspectives on nanostructural inhomogeneity in polymer network gels. Prog. Polym. Sci. **66**, 1–21 (2017)
39. Cannara, R.J., Eglin, M., Carpick, R.W.: Lateral force calibration in atomic force microscopy: a new lateral force calibration method and general guidelines for optimization. Rev. Sci. Instrum. **77**, 053701 (2006)
40. Johnson, K.L., Kendall, K., Roberts, A.D.: Surface energy and the contact of elastic solids. Proc. R. Soc. A **324**, 301–313 (1997)
41. Hertz, H.: Ueber die Berührung fester elastischer Körper. 156–171 (1882)
42. Gombert, Y., Simič, R., Roncoroni, F., Dübner, M., Geue, T., Spencer, N.D.: Structuring hydrogel surfaces for tribology. Adv. Mater. Interfaces **6**, 1901320 (2019)
43. Priya, M.V., Kumar, R.A., Sivashanmugam, A., Nair, S.V., Jayakumar, R.: Injectable amorphous chitin-agarose composite hydrogels for biomedical applications. J. Funct. Biomater. **6**, 849–862 (2015)
44. Hu, Z., Hong, P.Z., Li, S.D., Yang, L., Xie, J.Y.: Study on the preparation of quaternized chitosan/agarose microspheres for berbamine delivery. J. Polym. Mater. **29**, 361–370 (2012)
45. Godwin Uranta, K., Rezaei-Gomari, S., Russell, P., Hamad, F.: Studying the effectiveness of polyacrylamide (PAM) application in hydrocarbon reservoirs at different operational conditions. Energies **11**, 2201 (2018)
46. Wang, F.C., Feve, M., Lam, T.M., Pascault, J.P.: FTIR analysis of hydrogen bonding in amorphous linear aromatic polyurethanes. I. Influence of temperature. J. Polym. Sci. Part B: Polym. Phys. **32**, 1305–1313 (1994)
47. Dai, B., Matsukawa, S.: Elucidation of gelation mechanism and molecular interactions of agarose in solution by 1H NMR. Carbohydr. Res. **365**, 38–45 (2013)
48. De Gennes, P.G.: Scaling concepts in polymer physics. Cornell University Press, Ithaca and London (1979)
49. Shoaib, T., Carmichael, A., Corman, R.E., Shen, Y., Nguyen, T.H., Ewoldt, R.H., et al.: Self-adaptive hydrogels to mineralization. Soft Matter **13**, 5469–5480 (2017)
50. Delavoipiere, J., Tran, Y., Verneuil, E., Heurtefeu, B., Hui, C.Y., Chateauminois, A.: Friction of poroelastic contacts with thin hydrogel films. Langmuir **34**, 9617–9626 (2018)
51. Reale, E.R., Dunn, A.C.: Poroelasticity-driven lubrication in hydrogel interfaces. Soft Matter **13**, 428–435 (2017)
52. Watase, M., Nishinari, K.: Thermal and rheological properties of agarose-dimethyl sulfoxide-water gels. Polym. J. **20**, 1125–1133 (1988)
53. Deguchi, S., Lindman, B.: Novel approach for the synthesis of hydrophobe modified polyacrylamide. Direct N-alkylation of polyacrylamide in dimethyl sulfoxide. Polymer **40**, 7163–7165 (1999)
54. Brayton, C.F.: Dimethyl sulfoxide (DMSO): a review. Cornell Vet. **76**, 61–90 (1986)

55. Kirchner, B., Reiher, M.: The secret of dimethyl sulfoxide-water mixtures. A quantum chemical study of 1DMSO-nwater clusters. J. Am. Chem. Soc. **124**, 6206–6215 (2002)
56. Murat Ozmen, M., Okay, O.: Formation of macroporous poly(acrylamide) hydrogels in DMSO/water mixture: transition from cryogelation to phase separation copolymerization. React. Funct. Polym. **68**, 1467–1475 (2008)
57. Ozmen, M.M., Dinu, M.V., Okay, O.: Preparation of macroporous poly(acrylamide) hydrogels in DMSO/water mixture at subzero temperatures. Polym. Bull. **60**, 169–180 (2007)
58. LeBel, R.G., Goring, D.A.I.: Density, viscosity, refractive index, and hygroscopicity of mixtures of water and dimethyl sulfoxide. J. Chem. Eng. Data **7**, 100–101 (2002)
59. Rudge, R.E.D., Scholten, E., Dijksman, J.A.: Natural and induced surface roughness determine frictional regimes in hydrogel pairs. Tribol. Int. **141**, 105903 (2020)
60. Baumberger, T., Caroli, C., Ronsin, O.: Self-healing slip pulses along a gel/glass interface. Phys. Rev. Lett. **88**, 075509 (2002)
61. Hayashi, A., Kanzaki, T.: Swelling of agarose gel and its related changes. Food Hydrocolloids **1**, 317–325 (1987)
62. Xiong, J.Y., Narayanan, J., Liu, X.Y., Chong, T.K., Chen, S.B., Chung, T.S.: Topology evolution and gelation mechanism of agarose gel. J. Phys. Chem. B **109**, 5638–5643 (2005)
63. Gombert, Y., Roncoroni, F., Sanchez-Ferrer, A., Spencer, N.D.: The hierarchical bulk molecular structure of poly(acrylamide) hydrogels: beyond the fishing net. Soft Matter **16**, 9789–9798 (2020)
64. de Gennes, P.-G.: Effect of cross-links on a mixture of polymers. J. Physique Lett. **40**, 69–72 (1979)
65. Nakajima, T., Furukawa, H., Tanaka, Y., Kurokawa, T., Gong, J.P.: Effect of void structure on the toughness of double network hydrogels. J. Polym. Sci. Part B: Polym. Phys. **49**, 1246–1254 (2011)
66. Pitenis, A.A., Sawyer, W.G.: Lubricity of high water content aqueous gels. Tribol. Lett. **66**(3), 1–7 (2018)
67. Shoaib, T., Heintz, J., Lopez-Berganza, J.A., Muro-Barrios, R., Egner, S.A., Espinosa-Marzal, R.M.: Stick-slip friction reveals hydrogel lubrication mechanisms. Langmuir **34**, 756–765 (2018)
68. Cuccia, N.L., Pothineni, S., Wu, B., Mendez Harper, J., Burton, J.C.: Pore-size dependence and slow relaxation of hydrogel friction on smooth surfaces. Proc. Natl. Acad. Sci. USA **117**, 11247–11256 (2020)
69. McGhee, E.O., Chau, A.L., Cavanaugh, M.C., Rosa, J.G., Davidson, C.L.G., Kim, J., et al.: Amphiphilic gel lubrication and the solvophilic transition. Biotribology **26**, 100170 (2021)
70. Chen, Q., Wei, D., Chen, H., Zhu, L., Jiao, C., Liu, G., et al.: Simultaneous enhancement of stiffness and toughness in hybrid double-network hydrogels via the first physically linked network. Macromolecules **48**, 8003–8010 (2015)

Publisher's Note Springer Nature remains neutral with regard to jurisdictional claims in published maps and institutional affiliations.